Volt/Var Control and Energy Management in Non-Interconnected Insular Networks with Multiple Hybrid Power Plants

Evangelos E. Pompodakis[‡],   Georgios C. Kryonidis[†],   Emmanuel S. Karapidakis[**]

‡ Institute of Energy, Environment and Climatic Change, Hellenic Mediterranean University, Greece
† School of Electrical and Computer Engineering, Aristotle University of Thessaloniki, Greece
**School of Engineering, Power Systems and Energy Engineering, Hellenic Mediterranean University, Greece

Abstract—**This paper proposes a sensitivity-based optimization approach for the energy management and volt/var control of islanded networks powered by a thermal generator and several hybrid power plants (HPPs). Specifically, the method optimizes, in a 24-hour horizon, the active and reactive power of the HPPs, the output voltage of the thermal generator, as well as the settings of local voltage controllers e.g., step voltage regulators, capacitor banks, in order to minimize the generation cost of thermal generators and satisfy the following constraints: a) the technical limits of the diesel generators, b) the maximum direct penetration limits of the renewables, c) the state of charge limits of energy storage systems, d) the three-phase voltage limits of all the buses of the network. Simulations were executed in a modified islanded version of the IEEE 8500-node network, consisting of a diesel generator and multiple HPPs with various renewable generators and storage devices. According to the simulations, the proposed method minimizes the generation cost of diesel generators, while satisfying all the aforementioned technical constraints. In contrast to the existing optimization methods e.g., PSO, MINLP, which are practically inapplicable in large networks with a 24-hour optimization horizon, the proposed method presents very low computation time.**

Index Terms— **Energy management, energy storage systems, hybrid power plants, non-interconnected insular systems, optimization, sensitivity theory, volt/var control.**

NOTATIONS

Every variable with an arrow, e.g. $\vec{X}$, is a complex number.
Every variable without an arrow, e.g, X, is a real number.
The variables in bold, e.g., ***X***, *are vectors or matrices.*
$| \cdot |$ *denotes absolute value*
real $(\vec{X})$ *denotes the real part of* $\vec{X}$
imag $(\vec{X})$ *denotes the imaginary part of* $\vec{X}$
max (***X***) *denotes the maximum absolute value of vector* ***X***
min (***X***) *denotes the minimum absolute value of vector* ***X***
min (x, y) *returns the lowest value between numbers x and y*

I. INTRODUCTION

A. Background

ENERGY supply of non-interconnected islands is characterized by high levels of dependency and increased generation cost, mainly, due to the use of thermal generators operating with imported fossil fuels [1]. Nevertheless, islands exhibit increased wind and solar potential, which is rarely met in the mainland [2]. For example, Greece has more than 100 inhabited islands experiencing annual average wind velocities around 10 m/s, and solar irradiance around 1700 kwh/m² [2, Table 3]. Therefore, renewable energy sources (RESs) can be used in non-interconnected insular systems to reduce: a)

electricity generation cost, b) dependency on the imported fossil fuels, and c) CO_2 emissions. However, non-interconnected insular systems are usually small or medium size weak networks, where network operators apply strict operating constraints to ensure the secure and reliable grid operation [2],[3]. Specifically, thermal power plants should always operate above their technical minima [4]. Thus, in case of high RES production and low load demand, RES generation should be curtailed to avoid the violation of this constraint [2], [5]-[7]. Moreover, the advent of inertia-less and intermittent RES has affected the dynamic performance of weak non-interconnected networks [45]. Therefore, to ensure grid stability, network operators impose a maximum permissible limit in the direct (without storage) penetration of RES, known as dynamic RES penetration limit, curtailing any excess of renewable energy [2],[3],[5]-[7]. Consequently, the introduction of these technical limits hinders the further increase of RES penetration, discouraging also new investments.

Over the last years, there is a growing research and investment interest towards the installation of hybrid power plants (HPPs), for storing the excess renewable power, which otherwise would have been curtailed [1]-[2], [5]. An HPP is a cluster of RESs and storage systems, that operate in a coordinated way, thus forming a virtual power plant with controllable output power. With the installation of HPPs, a total annual RES penetration near to 90% can be achieved both for small and large islands [2], [8].

B. Literature Review

Volt/Var control (VVC) constitutes the cornerstone of the distribution management system (DMS). Its distinct feature is the ability to optimally coordinate local voltage controllers (LVCs), e.g., step voltage regulators (SVRs), switched capacitors, reactive power of the distributed generators (DGs), etc., in order to address possible voltage violations, while also achieving system-wide optimization objectives, e.g., loss minimization. Volt/Var control is executed by employing optimization-based techniques. Specifically, authors in [9] and [10] propose a sensitivity-based discrete coordinate-descent and a mixed integer linear programming (MILP), respectively, to reduce the voltage violations and power losses of distribution networks. However, these methods use single time instant horizon analysis. Thus, they are not applicable in networks with storage systems, where the optimization problem should be solved in a multiple time instant horizon to include the effective energy management of the storage systems. Considering the energy management of non-interconnected networks, the authors in [1],[2] propose a rule-based approach to actively

control the energy storage systems (ESSs) of the HPPs. However, the network operating constraints, e.g., voltage limits, are neglected in the conducted analyses. Additionally, ESSs are exploited in a non-optimal way since the stored energy is exploited, at each time instant, to the maximum possible extent, ignoring the future energy needs of the network. The optimal exploitation of ESSs is considered in [12], where a MILP problem is solved to minimize the generation cost of the islanded network, without, however, considering the network operating constraints e.g., voltage violations.

In [13] and [14], two methods are proposed that optimize the efficiency of DGs and power losses of the network, respectively. Nevertheless, energy management of ESS and is not considered in none of these methods. Finally, extremely small islanded microgrids were considered in both methods, raising questions about their applicability in large, islanded networks with multiple HPPs. In [15], [16] and [17], the authors apply artificial bee colony (ABC), genetic algorithm (GA) and mixed-integer optimization to optimize the operation cost of islanded microgrids in a given time horizon. However, Volt/Var techniques are missing, making the applicability of these methods problematic in large insular networks with voltage violations.

The authors in [24] and [25] apply heuristic optimization algorithms to minimize the operation cost of islanded MGs, eliminating also the voltage violations of the network. However, the computation time of heuristic optimization algorithms is extremely high when applied in large islanded unbalanced networks.

Authors in [18]-[22] use a mixed integer non-linear programming (MINLP) formulation to describe the optimization problem of an islanded microgrid (MG). To overcome the extremely long computation time of MINLP, non-linear equations are linearized, deriving a mixed integer linear programming (MILP) formulation. However, linear formulations cannot fully represent the nonlinearity of the power system, and therefore suffer some inherent inaccuracy [27]. Furthermore, based on the findings of [9], MILP can result in increased computation time when applied in large networks.

In [23], an algorithm to compute the energy management of storage devices in microgrids is proposed. However, its main drawback is the excessive computation time when applied in large networks with many storage devices [23]. The authors in [26] proposed a rule-based approach to allow battery units with low state-of-charge (SoC) to keep charging, while other batteries meet the demand. Nevertheless, the method does not guarantee optimal operation, e.g. minimization of thermal generation cost, as well as the voltage regulation of the network.

Finally, with the exception of [1], [2], [12], none of the aforementioned studies represent, accurately, the dynamic RES penetration limits, the technical limits of thermal generators as well as the operational modes of HPPs in non-interconnected insular networks. A summary of the basic features of the aforementioned methods is quoted in Table IV.

C. Main Contributions

This paper has been inspired by the sensitivity-based discrete coordinate-descent approach of [9]. However, significant improvements were made in order to execute, accurately and efficiently, the energy management and Volt/Var control of non-interconnected insular networks supplied by thermal generators and HPPs. The distinct features of the method are the following:

- It considers the network and load unbalances, which improves, significantly, the accuracy of the optimization problem, as pointed out in [18].
- It applies sensitivities to reduce the computation time of the method, even in very large insular networks.
- The technical limits of thermal generators and dynamic RES penetration limits are considered in the optimization.
- It optimizes the generation cost of thermal generators, by performing 24-hour energy management of HPPs as well as Volt/Var control for voltage regulation.

The rest of the paper is structured as follows: Section II categorizes the HPPs depending on their characteristics. Section III presents the power flow solver. Section IV presents the proposed optimization approach. Section V investigates the performance of the proposed approach via simulation results, while Section VI concludes the paper.

II.   CATEGORIZATION, CONNECTION AND MODELING OF HPPs

A. Categorization of HPPs

Non-interconnected insular networks suffer from large frequency deviations, after disturbances (e.g., a sudden loss of intermittent renewable power), often in excess of ±1 Hz, which could threaten the stability of insular networks [3],[28],[29]. To overcome this issue, a maximum dynamic RES penetration limit is imposed by the network operator (around 30% of the network's load, in Greece [1],[3],[6],[29] and other countries [46]), curtailing the excess renewable power.

HPPs can be utilized to increase the renewable's penetration in insular networks [1] [2] and reduce curtailments, by storing a large part or the whole renewable power and injecting it through dispatchable generators. HPPs are categorized in four categories, depending on the response time of ESS, as shown in Fig. 1 at the end of the paper:

a) *Pumped Hydroelectric Storage (PHS)*: It consists of two water reservoirs at different elevations, connected through two penstocks, as shown in Fig. 1a [1] [2]. Due to the relative slow response of PHS (higher than 20 sec according to [30, Table 8] and [41, Fig. 7]), they are not able to compensate, instantaneously, the renewable's fluctuations [1] [2]. As a result, the direct penetration of renewables in HPPs with PHS is discouraged [1][2][39].

b) *Hydrogen Storage Systems (HSS)*: Similar to PHS, fuel cells present a slow response, and therefore, the direct penetration of renewables is discouraged. The renewable power is stored in the form of hydrogen [44], which produces power through fuel cells, in a controllable way.

c) *Battery Storage Systems (BSS)*: In case of electrochemical storage, the direct penetration of renewables can be as high as 100% [1] [2] [31], due to the instantaneous response of batteries[1] (around 1 sec [30, Table 7]). Therefore, BSS[2] can be used as a mean to compensate, instantaneously, a sudden renewable power loss [1][12], and thus, preventing unacceptable frequency oscillations that can cause

---

[1] Super capacitors and flywheels belong to the same category with BSS due to their very fast response [30].

[2] Either new or retired batteries from electric vehicles [11].

subsequent load shedding or generator outages [3][42][43][45].

d) *Compressed Air Energy Storage (CAES):* Similar to PHS and HSS, CAES present a slow response time [30, Table 8], and therefore, the direct penetration of renewables is discouraged, as well.

B. Internal Connection of Renewables in HPPs

Depending on the internal connection of renewables, inside the HPP, the following connection modes are distinguished:

a) *Mode 1: All renewables are connected to the grid.* All the renewables of HPP are directly connected to the grid, as shown in Fig. 1c. This kind of connection is encouraged only in HPPs with fast storage systems e.g., batteries [12], super capacitors, flywheels, which are able to provide, instantaneously, power reserves after large renewable's fluctuations [1] [2]. On the opposite, in HPPs with slow ESSs, this connection mode is examined with skepticism by the island system operator [39].

b) *Mode 2: All renewables are connected to the storage system.* In this connection mode, all the renewables inside the HPP are indirectly connected to grid via the storage system acting as an intermediate layer. This connection mode is recommended for HPPs with slow response time (e.g., PHS, HSS, CAES) connected to saturated networks with a high generation of intermittent sources. With respect to Figs. 1a, 1b, 1d, it practically means $P_{dp_{hppi}}(t) = 0$ and $P_{resi}(t) = P_{chrg_{hppi}}(t) \quad \forall i \in \{1,2,4\}$ and $t \in \{0,1,\dots23\}$, where $P_{dp_{hppi}}(t)$, $P_{resi}(t)$ and $P_{chrg_{hppi}}(t)$ is the direct penetration, the power generated by the renewables and the charging power of the storage system of HPP i at time t. This connection mode does not pose any challenge to the dynamic stability of the grid since the HPP injects only non-intermittent power by the storage system. To compensate the round-trip losses of ESS, economic incentives are given to the owners of HPPs, selling the stored energy at higher tariffs than the direct wind energy [39, Table I][3]. This policy, although it increases energy losses, it also increases the HPP owner's profit and also benefits the System Operator, by providing dispatchable renewable power and reserves, through which some of the uncertainty of the external wind farms can be managed [39].

c) *Mode 3: Renewable units of HPP are split.* More specifically, a number of renewable units are connected directly to the grid, while the rest are connected to the grid via the storage system acting as an intermediate layer. This connection mode is suitable in case of unsaturated islands with low wind penetration and sufficient dynamic stability margin for accepting, directly, additional renewable power. Assuming that α_{dpi} is the percentage of renewable units of HPP i connected directly to the grid, the powers of Figs. 1a, 1b, and 1d are calculated as: $P_{dp_{hppi}}(t) = \alpha_{dpi} \cdot P_{resi}(t)$ and $P_{chrg_{hppi}}(t) = (1 - \alpha_{dpi}) \cdot P_{resi}(t) \quad \forall i \in \{1,2,4\}$ and $t \in \{0,1,\dots23\}$. The benefit of this connection is that the renewable units that are directly connected to the grid are not subject to round-trip storage losses. However, a portion

of this power will may be required to be curtailed in periods of low load demand and high renewable production, in order to ensure the dynamic RES penetration limit.

C. Modelling the Voltage Profile of HPPs

As shown in Fig. 1, the generators of HPPs can be a) synchronous generators (SG) e.g., Hydroturbines, turbines of CAES, b) inverter-based distributed generators (IBDG) e.g., photovoltaics, batteries, fuel cells, type IV wind generator, c) asynchronous generators e.g., type I and II wind turbines, d) type III wind generator or Double fed induction generators (DFIG). A synchronous generator generates a balanced phase-to-neutral (in 4-wire grids) or phase-to-phase (in 3-wire grids) voltage[4], even under unbalanced loading conditions. Also, IBDGs with their flexible control generate a balanced voltage. According to Fig. 1, all HPPs comprise at least one generator with voltage balancing capability, namely either a SG or an IBDG, and therefore, we consider, with a good accuracy, that all HPPs generate a balanced voltage profile. Owing to the balanced voltage profile of HPPs, their negative- and zero-sequence powers are zero, and thus, in Fig.1, the variables $P_{dschrg_{hppi}}(t)$ and $P_{dp_{hppi}}(t) \ \forall i \in \{1, \dots, 4\}$ and $t \in \{0, 2, \dots, 23\}$, denote positive sequence powers.

III. POWER FLOW SOLVER

For the implementation of our approach, a three-phase power flow solver is required, which should accommodate the following characteristics: a) fast computation time, b) accurate modelling of SVRs and capacitor banks, c) precise representation of balanced buses in order to accurately model the balanced voltage of HPPs. In this paper we used the implicit Z-Bus power flow method proposed in [35], which fulfills the aforementioned requirements. However, other solvers could be used as well e.g., current injection, Newton Raphson, Fortescue decomposition, Gauss-Seidel, provided that they fulfill the aforementioned requirements.

In [35], a model was developed which separates the sequence components of DGs. More specifically, the positive-sequence component is modeled through current sources, while the negative- and zero-sequence components are modeled through admittances (Y_0, Y_2) that are incorporated in the admittance matrix of the network. To model the voltage balancing capabilities of HPPs, $Y_0 = Y_2 \to \infty$ in four-wire networks, while $Y_2 \to \infty$ in three wire networks [35]. For the incorporation of the SVRs in the power flow, we used the model of [33].

IV. PROPOSED CONTROL ALGORITHM

To explain the mathematical formulation of our approach, let us assume an MV insular network, which is supplied by a thermal generator (assumed as a slack bus), the four HPPs of Fig.1, a wind farm (WF), a SVR, and a capacitor bank. The schematic of the example network is shown in Fig. 2.

A. Initialization of the 24-h Optimization Problem

---

[3] The regulatory framework of Greece for HPPs was modified in 2016. However, the basic idea of higher pricing of stored energy remains in the new framework, as well [40]. Specifically, according to article 21 of [40], energy generated from ESSs is compensated 50% higher than direct wind power.

[4] SG units inherently present nonzero finite negative- and zero-sequence admittances [35]. However, they are very small, and thus, with a sufficient accuracy, SG units can be considered to generate balanced voltage, as confirmed by the results of Tables III-Table VII in [38].
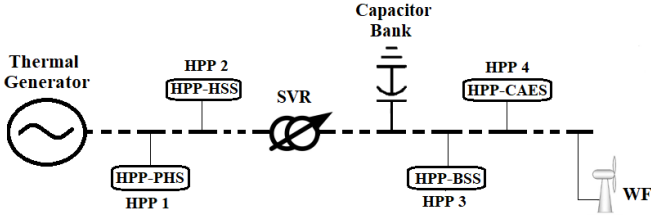
Fig. 2. Schematic diagram of the example network.

As a first step, the direct penetration of the WF and the HPPs, for each time interval $t \in \{0, 1,..., 23\}$ is determined. In the absence of storage, WF has a priority to cover the 30 % margin of direct penetration. The rest is shared to the HPP 1, HPP 2, and HPP 4. HPP 3 injects all the renewable power to the grid due to the fast response of BSS, which can compensate the fast renewable power variations. The wind direct penetration of the HPP $i \in \{1, 2, 4\}$, for the time interval t, is mathematically calculated by (1a). The wind direct penetration of the HPP 3, for the time interval t, is mathematically calculated by (1b).

$$P_{dp_{hppi}}(t) = min\left(\left(0.3 \cdot P_{load}(t) - P_{wf}(t)\right) \cdot \frac{\alpha_{dpi} \cdot p_{ri}}{\alpha_{dp1} \cdot p_{r1} + \alpha_{dp2} \cdot p_{r2} + \alpha_{dp4} \cdot p_{r4}} \cdot u\left(0.3 \cdot P_{load}(t) - P_{wf}(t)\right), \alpha_{dpi} \cdot P_{resi}(t)\right)$$
(1a)

$$P_{dp_{hpp3}}(t) = P_{res3}(t)$$
(1b)

Here, $P_{dp_{hppi}}(t)$ is the power directly injected to the grid from HPP $i = \{1, 2, 3, 4\}$ at time interval t. $P_{load}(t)$ is the total load of the network at time interval t. $P_{wf}(t)$ is the power generated by the WF at time t. p_{ri} is the nominal installed power of renewables of HPP i. $P_{resi}(t)$ is the generated power from the renewables of the HPP i at time t. α_{dpi} is the percentage of renewables connected directly to the network as defined in Section II.B. u is the step function. The function $min(x, y)$ returns the lowest value between x and y.

The charge power of the storage system of HPP $i \in \{1, 2, 4\}$ and HPP 3, for the time interval t, are expressed by (2a) and (2b), respectively:

$$P_{chrg_{hppi}}(t) = P_{resi}(t) \cdot (1 - \alpha_{dpi})$$
(2a)

$$P_{chrg_{hpp3}}(t) = 0$$
(2b)

where $P_{chrg_{hppi}}(t)$ is the charge power of HPP i, at time interval $t \in \{0, 1, ..., 23\}$. $P_{chrg_{hppi}}(t)$, $P_{resi}(t)$ are depicted on Fig. 1.

The optimization approach is initialized by setting the discharge power of the storage systems of HPP $i \in \{1, 2, 4\}$ and HPP 3, according to (3):

$$P_{dschrg_{hppi}}(t) = \varepsilon_{chrgi} \cdot \varepsilon_{dschrgi} \cdot P_{chrg_{hppi}}(t)$$
(3a)

$$P_{dschrg_{hpp3}}(t) = 0$$
(3b)

where ε_{chrgi} and $\varepsilon_{dschrgi}$ is the charge and discharge efficiency of the storage system of HPP i, respectively. It is noted that setting, initially, the discharge powers of the storage systems of HPPs according to (3), their stored energy remains unchanged, since the output powers of the storage systems are equal to the input ones.

B. Mathematical Formulation of the 24-h Horizon Optimization Problem

The control variables of the proposed multi-objective optimization approach, for the network of Fig. 2, are the following:
- $P_{dschrg_{hpp1}}(t), P_{dschrg_{hpp2}}(t), P_{dschrg_{hpp3}}(t), P_{dschrg_{hpp4}}(t)$ $\forall t \in \{0, ..., 23\}$ hours,
- $Q_{hpp1}(t), Q_{hpp2}(t), Q_{hpp3}(t), Q_{hpp4}(t)$ $\forall t \in \{0, ..., 23\}$, where $Q_{hppi}(t)$ is the reactive power generated by the HPP $i = \{1, 2, 3, 4\}$ at time interval t.
- $Tap_{kr}(t)$ where $k = \{1, ..., N_{svr}\}$, N_{svr} is the number of SVRs (1 in Fig. 2). r is the phase of SVR such that $r = \{a, b, c\}$.
- $Cap_{lr}(t)$ where $l = \{1, ..., N_{cap}\}$, N_{cap} is the number of capacitor banks (1 in Fig. 2). r is the phase of capacitor bank such that $r = \{a, b, c\}$.

The optimization objectives are the following:
- *Objective 1*: Minimization of the generated power of the thermal power plant, satisfying the technical limits ($TechLim$) of thermal generator,
- *Objective 2*: Forcing the difference between maximum and minimum network's voltage below a threshold ($VoltLim$).

The mathematical formulation of the cost function (Cost) is given in (4), where $Horizon = 23$, for a 24-hour optimization.

$$Cost = \sum_{t=0}^{Horizon} c_{obj1} \cdot \left[real\left(V_0(t) \cdot Y_{0,1} \cdot (V_0(t) - V_1(t) - dV_1(t))\right) - TechLim\right]^2 +$$

$$\sum_{t=0}^{Horizon} c_{obj2} \cdot \left[max(V(t) + dV(t)) - min(V(t) + dV(t)) - VoltLim\right]^2 \cdot u\left(max(V(t) + dV(t)) - min(V(t) + dV(t)) - VoltLim\right)$$

(4)

In (4), c_{obj1}, c_{obj2} are the penalty coefficients of the *objective 1* and *objective 2*, respectively. $V_0(t)$ is the voltage of the thermal generator (slack) at time interval t, such that $V_0(t) = \left[\overrightarrow{V_{0a}(t)} \quad \overrightarrow{V_{0b}(t)} \quad \overrightarrow{V_{0c}(t)}\right]^T$, where $\overrightarrow{V_{0r}(t)}$ is the phase voltage of phase $r = \{a, b, c\}$ of slack bus. $Y_{0,1}$ is the admittance matrix of the line connecting the slack bus with its neighboring bus (bus 1). $V_1(t)$ is the voltage vector of bus 1 at time interval t, such that $V_1(t) = \left[\overrightarrow{V_{1a}(t)} \quad \overrightarrow{V_{1b}(t)} \quad \overrightarrow{V_{1c}(t)}\right]^T$, where $\overrightarrow{V_{1r}(t)}$ is the voltage of phase $r = \{a, b, c\}$ of bus 1. $TechLim$ is the technical minima of thermal generator. $dV_1(t)$ is the variation of the voltage vector of bus 1, $\forall t \in \{0, ..., 23\}$, due to the variations of

control variables $P_{dschrg_{hppi}}(t)$, $Q_{hppi}(t)$, $Cap_{lr}(t)$, $Tap_{kr}(t)$. $V(t) = [V_1(t) \quad ... \quad V_m(t)]^T$ contains the voltage vectors of all the buses of the network. $dV(t)$ is the variation of the vector $V(t)$ due to the variation of control variables. The functions $max(V(t))$ and $min(V(t))$ return respectively the maximum and minimum absolute value of vector $V(t)$ $\forall t \in \{0, ..., 23\}$. $VoltLim$ is the maximum allowable deviation between the upper and lower voltage limits.

The *objective 1* is achieved from the first term of (4). It is clarified that the term $real\left(V_0(t) \cdot Y_{0,1} \cdot (V_0(t) - V_1(t) - dV_1(t))\right)$ denotes the active power (real part) generated by the thermal

generator (slack bus 0) at time interval t. Therefore, $real\left(\boldsymbol{V_0}(t) \cdot \boldsymbol{Y_{0,1}} \cdot \left(\boldsymbol{V_0}(t) - \boldsymbol{V_1}(t) - \boldsymbol{dV_1}(t)\right)\right) - TechLim$ denotes the deviation of the active power of thermal generator from its technical minima $\forall\, t \in \{0, \dots, 23\}$. During the high load hours, the storage systems of HPPs are forced to discharge to reduce the cost function, and thus, the consumption of fossil fuel and CO_2 emissions. On the opposite, during low load hours, to avoid operating thermal generator below its technical minima, the storage systems of HPPs are forced to be charged so that the thermal generator operates exactly at its technical minima.

The *objective 2* forces the deviation between the maximum and minimum voltage of the network, $\forall\, t \in \{0, \dots, 23\}$, to be below a threshold value $VoltLim$. It is noted that *objective 2*, by itself, does not ensure the compliance of allowable voltage limits e.g., $\pm 5\%$. To make it clear, let us assume an MV network with a phase-to-neutral voltage 7200 V and maximum allowable voltage range $\pm 5\%$, namely all bus voltages should range between 6840V and 7560V. *Objective 2* ensures that the deviation between maximum and minimum voltage will be less than 720 V ($10\% \cdot 7200$V) $\forall\, t \in \{0, \dots, 23\}$, but not all voltages will lie inside 6840V and 7560V. For this reason, additional control actions are required, by regulating the voltage of thermal generator through automatic voltage regulators (AVRs) until all voltages lie inside their limits. More details about the regulation of AVR are provided in step 5 of Section IV.E.

C. Derivation of Sensitivity Parameters

In this sub-section, the sensitivity of $\boldsymbol{V}(t)$ from the control variables is defined. More specifically, we present the derivative $\frac{\partial V(t)}{\partial X_{cv}(t)}$, where $X_{cv}(t) \in \left\{ P_{dschrg_{hppi}}(t)\ Q_{hppi}(t)\ Tap_{kr}(t)\ Cap_{lr}(t) \right\}$ is the control variable at time t. Scope in every repetition of the optimization is to find the optimal $dX_{cv}(t)\ \forall\, t \in \{0, \dots, 23\}$, which result in the best $\boldsymbol{dV}(t) = \frac{\partial V(t)}{\partial X_{cv}(t)} \cdot dX_{cv}(t)$ and $\boldsymbol{dV_1}(t) = \frac{\partial V_1(t)}{\partial X_{cv}(t)} \cdot dX_{cv}(t)$ that minimize the cost function (4).

Firstly, it is necessary to define the impedance matrix of the network ($\boldsymbol{Z_{matr}}$), as follows:

$$\boldsymbol{Z_{matr}} = \begin{bmatrix} Z_{1,1} & \cdots & Z_{1,m} \\ \vdots & \ddots & \vdots \\ Z_{m,1} & \cdots & Z_{m,m} \end{bmatrix} \tag{5}$$

where m is the number of buses, the element $\boldsymbol{Z_{i,j}}$ of $\boldsymbol{Z_{matr}}$ is denoted in (6). In fact, $\boldsymbol{Z_{matr}}$ is the inverse of the admittance matrix of the network, namely $\boldsymbol{Z_{matr}} = \left(Y_{fin2}^{ac} \right)^{-1}$, where Y_{fin2}^{ac} has been defined in [35, eq. (13)].

$$\boldsymbol{Z_{i,j}} = \begin{bmatrix} \overrightarrow{Z_{ia,ja}} & \overrightarrow{Z_{ia,jb}} & \overrightarrow{Z_{ia,jc}} \\ \overrightarrow{Z_{ib,ja}} & \overrightarrow{Z_{ib,jb}} & \overrightarrow{Z_{ib,jc}} \\ \overrightarrow{Z_{ic,ja}} & \overrightarrow{Z_{ic,jb}} & \overrightarrow{Z_{ic,jc}} \end{bmatrix} \tag{6}$$

i. Derivation of $\frac{\partial V(t)}{\partial P_{dschrg_{hppi}}(t)}$

Assuming that HPP i is connected to bus z, then the derivative $\frac{\partial V(t)}{\partial P_{dschrg_{hppi}}(t)}$ is calculated by (7):

$$\frac{\partial V(t)}{\partial P_{dschrg_{hppi}}(t)} = \begin{bmatrix} Z_{1,z} \\ \cdots \\ Z_{m,z} \end{bmatrix} \cdot \begin{bmatrix} 1 \\ \alpha^2 \\ \alpha \end{bmatrix} \cdot \frac{1}{\overrightarrow{V_z^+}(t)^*} \tag{7}$$

where $\overrightarrow{V_z^+}(t)^*$ is the complex conjugate of the positive-sequence voltage of bus z at time t. Parameter α is a phasor rotation operator such that $a = e^{j\frac{2}{3}\pi}$. Note that in (7), the term

$[1\quad \alpha^2\quad \alpha]^T \cdot 1/\overrightarrow{V_z^+}(t)^*$ expresses the variation of the positive-sequence current of HPP i due to the step variation of the positive-sequence power ($P_{dschrg_{hppi}}$).

ii. Derivation of $\frac{\partial V(t)}{\partial Q_{hppi}(t)}$

Assuming that HPP i is connected to bus z, then the derivative $\frac{\partial V(t)}{\partial Q_{hppi}(t)}$ is calculated by (8):

$$\frac{\partial V(t)}{\partial Q_{hppi}(t)} = \begin{bmatrix} Z_{1,z} \\ \cdots \\ Z_{m,z} \end{bmatrix} \cdot \begin{bmatrix} 1 \\ \alpha^2 \\ \alpha \end{bmatrix} \cdot \frac{e^{-j\frac{\pi}{2}}}{\overrightarrow{V_z^+}(t)^*} \tag{8}$$

iii. Derivation of $\frac{\partial V(t)}{\partial Tap_{kr}(t)}$

The 3-bus equivalent circuit of [33] is applied in this paper to model SVRs. It is depicted in Fig. 3, assuming that the SVR is connected between the buses p and s.

The equations of current sources are provided in [33, Table 3], while the admittances $\boldsymbol{Y_{pm}}, \boldsymbol{Y_{ms}}$ in [33, Table 2]. The tap variables are included in the current sources, thus avoiding the continuous factorization of the network's admittance matrix (Y_{fin2}^{ac}) after each change of taps. Furthermore, the inclusion of taps into the current sources enables the construction of sensitivity parameters relating the voltage with the current sources, as shown in (9).

$$\frac{\partial V(t)}{\partial Tap_{kr}(t)} = \begin{bmatrix} Z_{1,p} \\ \cdots \\ Z_{N_{bus},p} \end{bmatrix} \cdot \boldsymbol{dI_p} + \begin{bmatrix} Z_{1,m} \\ \cdots \\ Z_{N_{bus},m} \end{bmatrix} \cdot \boldsymbol{dI_m} + \begin{bmatrix} Z_{1,s} \\ \cdots \\ Z_{N_{bus},s} \end{bmatrix} \cdot \boldsymbol{dI_s} \tag{9}$$

where $\boldsymbol{dI_p}, \boldsymbol{dI_m}, \boldsymbol{dI_s}$ are formed according to [33, Table 3], depending on the configuration and type of SVR.
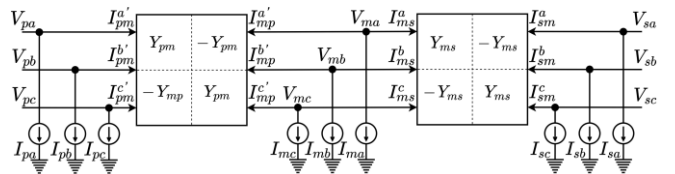
Fig. 3. The 3-bus equivalent circuit of an SVR connected between buses p and s [33]. Bus m is a fictitious bus, which is added to enhance the convergence of Z-Bus power flow [33].

iv. Derivation of $\frac{\partial V(t)}{\partial Cap_{kr}(t)}$

Assuming that capacitor bank k is connected to bus q, then the derivatives $\frac{\partial V(t)}{\partial Cap_{kr}(t)}$ are calculated by (10):

$$\frac{\partial V(t)}{\partial Cap_{kr}(t)} = \begin{bmatrix} \overrightarrow{Z_{1a,qr}} \\ \overrightarrow{Z_{1b,qr}} \\ \cdots \\ Z_{mc,qr} \end{bmatrix} \cdot e^{j\frac{\pi}{2}} \cdot \omega \cdot \overrightarrow{V_{qr}(t)} \tag{10}$$

where ω is the angular frequency of the network, $\overrightarrow{V_{qr}(t)}$ is the voltage of phase $r = \{a, b, c\}$ of bus q, m is the number of buses of the network, $\overrightarrow{Z_{ia,ja}}$ has been defined in (6).

D. Constraints of Control Variables

The control variables described in the previous sub-section should be constrained based on the physical properties of generators, storage systems of HPPs, SVRs and capacitor banks.

i. Constraints for HPPs

$$P_{dschrg_i}^{min} < P_{dschrg_{hppi}}(t) < P_{dschrg_i}^{max} \quad \forall \, t \in \{0, \dots, Horizon\} \quad (11)$$

$$S_{hpp_i}(t) < S_{hpp_i}^{max} \quad \forall \, t \in \{0, \dots, Horizon\} \quad (12)$$

$$StE_{hpp_i}^{min} < StE_{hpp_i}(t) + P_{chrg_{hppi}}(t) \cdot \varepsilon_{chrgi} + \frac{P_{dschrg_{hppi}}(t)}{\varepsilon_{dschrgi}} < StE_{hpp_i}^{max}$$
$$\forall \, t \in \{0, \dots, Horizon\} \quad (13)$$

In (11), $P_{dschrg_i}^{min}$ and $P_{dschrg_i}^{max}$ is the minimum and maximum discharge power of HPP i, respectively. Eq. (12) ensures that the apparent power of HPP i does not exceed the maximum apparent power $S_{hpp_i}^{max}$. Finally, eq. (13) ensures that the charge and discharge of HPP i will not cause an excess of the maximum ($StE_{hpp_i}^{max}$) and minimum ($StE_{hpp_i}^{min}$) stored energy. $StE_{hpp_i}(t)$ is the stored energy of HPP i in time interval t.

ii. Constraints for SVRs

$$Tap_k^{min} < Tap_{kr}(t) < Tap_k^{max}$$

$$\forall \, t \in \{0, \dots, Horizon\} \text{ and } r = \{a, b, c\} \quad (14)$$

Eq. (14) ensures that the tap setting of SVR k lies inside the maximum (Tap_k^{max}) and minimum (Tap_k^{min}) capacitor limits. Usually, $Tap_k^{max} = 16$ and $Tap_k^{min} = -16$ [33].

iii. Constraints for Capacitor Banks

$$0 < Cap_{lr}(t) < Cap_l^{max}$$

$$\forall \, t \in \{0, \dots, Horizon\} \text{ and } r = \{a, b, c\} \quad (15)$$

Eq. (15) ensures that the steps of capacitor bank l lie inside the maximum (Cap_l^{max}) and minimum (0) limits, for each time instant of the optimization horizon. Technical details about capacitor banks are provided in [34].

E. Steps of the Proposed Optimization Approach

The control variables of the optimization problem have been defined in Section IV.B and are divided in two groups: The *interdependent optimization variables* and the *non-interdependent optimization variables*.

a) *Interdependent optimization variables*: Assuming the network of Fig. 2, the interdependent optimization variables $Z = \{P_{dschrg_{hpp1}}(t), P_{dschrg_{hpp2}}(t), \ P_{dschrg_{hpp3}}(t), P_{dschrg_{hpp4}}(t)\}$ $\forall \, t \in \{0, \dots, 23\}$ are the discharge powers of the four HPPs. They are named interdependent because the discharge of HPP i at time instant t can affect the discharge capability of the same HPP at another time instant, due to its maximum/minimum stored energy (see constraint (13)). For example, if the ESS of HPP i is completely discharged during the first hours, there will not be sufficient stored energy to cover the peak demand of the next hours.

b) *Non-interdependent optimization variables*: The non-interdependent optimization variables $Y = \{Q_{hpp1}(t), Q_{hpp2}(t), Q_{hpp3}(t), Q_{hpp4}(t), Tap_{1a}, Tap_{1b}, Tap_{1c}, Cap_{1a}(t), Cap_{1b}(t), Cap_{1c}(t) \} \, \forall \, t \in \{0, \dots, Horizon\}$ are the reactive power of HPPs, the taps of SVR and the steps of capacitor bank. They are named non-interdependent since their action in time instant t do not affect their operation at future time instants.

Definitions: Define the step variations of control variables ($dp, dq, dTap, dCap$). dp, dq are arbitrarily selected. Small values of dp, dq may lead to a better final solution at the expense of reducing the convergence speed. $dTap$ is set equal to the tap of SVR e.g., 0.00625, while the $dCap$ is set equal to the step of capacitor bank. Moreover, we define the vectors $Best\_Variable \in \mathbb{R}^{1xHorizon}$ and $Best\_Action \in \mathbb{R}^{1xHorizon}$, which both have a dimension 1x*Horizon* and include respectively the best variable and action, which lead to the lowest *Cost* function in (4). For example, assuming that in the time interval $t=0$, the action $+dTap$ of the variable Tap_{1a} results in the lowest *Cost* value, then $Best\_Variable\,(0) = Tap_{1a}$ and $Best\_Action(0) = +dTap$. Similar for the other $t \in \{1, \dots, Horizon\}$.

The steps of the proposed optimization approach are defined below:

Initialization: Estimate the loads and renewables for the 24-hour horizon (the variable *Horizon=23*). Set the direct penetration and charge powers of HPPs from (1) and (2), respectively. Moreover, initialize the discharge powers of HPPs from (3). Solve the power flow $\forall \, t \in \{0, \dots, Horizon\}$, using the initialized values.

Step 1: Execute only one power flow iteration $\forall \, t \in \{0, \dots, Horizon\}$.

Step 2: Calculate the *Cost* value for each possible single action $+dp$ or $-dp$ or $+dq$ or $-dq$ or $+dTap$ or $-dTap$ or $+dCap$ or $-dCap$ of each control variable Z and Y, $\forall \, t \in \{0, \dots, Horizon\}$. In (4), $V(t)$ is calculated from step 1, while $dV(t)$ via the sensitivity parameters and the step variations of control variables e.g., $+dp$ etc. Actually, in this step, we predict, via sensitivities, the *Cost* function of all possible single actions of control variables, $\forall \, t \in \{0, \dots, Horizon\}$. Our goal is to find the best action $\forall \, t \in \{0, \dots, Horizon\}$ that will result in the minimization of *Cost* function.

Step 3: Update the $Best\_Variable(t)$ and $Best\_Action(t)$ vectors based on the optimal results of Step 2, $\forall \, t \in \{0, \dots, Horizon\}$. In that step, we save, in two vectors, the optimal variable e.g., $P_{dschrg_{hpp1}}, Q_{hpp1}, \forall \, t \in \{0, \dots, Horizon\}$, and their corresponding optimal action e.g., $+dp, -dq$ etc.

Step 4: Execute the optimal actions of all non-interdependent optimization variables in $Best\_Variable$ vector. Moreover, execute (only some) selected optimal actions of the interdependent optimization variables of $Best\_Variable$ vector. To make it clear, let us assume that $Best\_Variable = [P_{dschrg_{hpp1}} \ Q_{hpp2} \ Q_{hpp1} \ Q_{hpp3} \ Cap_{1a} \ Cap_{1b}$ $Q_{hpp4} \ Q_{hpp2} \ Tap_{1a} \ Tap_{1a} \ Tap_{1b} \ Tap_{1c} \ P_{dschrg_{hpp1}} \ P_{dschrg_{hpp1}}$ $Q_{hpp1} \ Q_{hpp1} \ Q_{hpp1} \ Q_{hpp2} \ P_{dschrg_{hpp3}} \ P_{dschrg_{hpp3}} \ P_{dschrg_{hpp2}} \ Q_{hpp4}$ $P_{dschrg_{hpp4}} \ Q_{hpp4}]$ and $Best\_Action = [+dp \ -dq \ +dq \ -dq$ $+dCap \ +dCap \ -dq \ -dq \ +dTap \ +dTap \ -dTap \ -dTap$ $+dp \ +dp \ -dq \ -dq \ +dq \ +dq \ +dp \ -dp \ -dp$ $+dq \ +dp \ +dq]$. The update of the interdependent and non-

interdependent optimization variables, for our example, is shown below, where k is the iteration of optimization algorithm.

<u>Executed actions of non-interdependent variables for the examined example at kth iteration</u>

$Q_{hpp2}(2)^{\kappa+1} = Q_{hpp2}(2)^\kappa - dq$

$Q_{hpp1}(3)^{\kappa+1} = Q_{hpp1}(3)^\kappa + dq$

$Q_{hpp3}(4)^{\kappa+1} = Q_{hpp3}(4)^\kappa - dq$

$Cap_{1a}(5)^{\kappa+1} = Cap_{1a}(5)^\kappa + dCap$

$Cap_{1b}(6)^{\kappa+1} = Cap_{1b}(6)^\kappa + dCap$

$Q_{hpp4}(7)^{\kappa+1} = Q_{hpp4}(7)^\kappa - dq$

$Q_{hpp2}(8)^{\kappa+1} = Q_{hpp2}(8)^\kappa - dq$

$Tap_{1a}(9)^{\kappa+1} = Tap_{1a}(9)^\kappa + dTap$

$Tap_{1a}(10)^{\kappa+1} = Tap_{1a}(10)^\kappa + dTap$

$Tap_{1b}(11)^{\kappa+1} = Tap_{1b}(11)^\kappa - dTap$

$Tap_{1c}(12)^{\kappa+1} = Tap_{1c}(12)^\kappa - dTap$

$Q_{hpp1}(15)^{\kappa+1} = Q_{hpp1}(15)^\kappa - dq$

$Q_{hpp1}(16)^{\kappa+1} = Q_{hpp1}(16)^\kappa - dq$

$Q_{hpp1}(17)^{\kappa+1} = Q_{hpp1}(17)^\kappa + dq$

$Q_{hpp2}(18)^{\kappa+1} = Q_{hpp2}(18)^\kappa + dq$

$Q_{hpp4}(22)^{\kappa+1} = Q_{hpp4}(22)^\kappa + dq$

$Q_{hpp4}(24)^{\kappa+1} = Q_{hpp4}(24)^\kappa + dq$

<u>Executed actions of interdependent variables for the examined example at kth iteration</u>

$P_{dschrg_{hpp1}}(1)^{\kappa+1} = P_{dschrg_{hpp1}}(1)^\kappa + dp$

$P_{dschrg_{hpp1}}(13)^{\kappa+1} = P_{dschrg_{hpp1}}(13)^\kappa + dp$

$P_{dschrg_{hpp1}}(14)^{\kappa+1} = P_{dschrg_{hpp1}}(14)^\kappa + dp$

> Execute (only) the best action, which leads to the lowest Cost

$P_{dschrg_{hpp3}}(19)^{\kappa+1} = P_{dschrg_{hpp3}}(19)^\kappa + dp$

$P_{dschrg_{hpp3}}(20)^{\kappa+1} = P_{dschrg_{hpp3}}(20)^\kappa - dp$

> Execute both actions since they are opposite and do not affect the total state-of-charge of HPP 3

$P_{dschrg_{hpp2}}(21)^{\kappa+1} = P_{dschrg_{hpp2}}(21)^\kappa - dp$

$P_{dschrg_{hpp4}}(23)^{\kappa+1} = P_{dschrg_{hpp4}}(23)^\kappa + dp$

> Execute both actions since they regard different HPPs

As shown, the optimal actions of non-interdependent variables are all executed, since an execution in time instant t does not affect their operation in future time instants. On the opposite, only the best discharge actions should be performed for the $P_{dschrg_{hpp1}}$. In this way, the stored energy of the ESSs is regarded as a resource to be optimally allocated along the 24-h horizon, and it is mostly disposed in time instants of higher demand.

Step 5: The slack voltage, $\forall\ t\ \in \{0, ..., Horizon\}$, is updated by $dV_{slack}(t)$, as follows:

$$dV_{slack}(t) = V_{nom} - \frac{max(\boldsymbol{V}(t)) + min(\boldsymbol{V}(t))}{2} \quad (16)$$

where V_{nom}, $max(\boldsymbol{V}(t)), min(\boldsymbol{V}(t))$ is the nominal, maximum and minimum voltage of the network at time t, respectively. As an example, let us consider a network with nominal voltage $V_{nom} = 7200V$ and allowable voltage limits of $6840V$ and $7560V$, respectively ($\pm5\%$). Let us further assume that the maximum and minimum voltages, at time t, have been forced from *objective 2* of (4) to be $max(\boldsymbol{V}(t)) = 7720\ V$ and $min(\boldsymbol{V}(t)) =$

$7000V$, respectively. Obviously, the maximum voltage limit is exceeded by 160V. Nevertheless, if the voltage of thermal generator is updated from (16) by $dV_{slack} = 7200 - \frac{7720 + 7000}{2} = -160V$, all network voltages will be reduced by 160 V, and thus, they will all lie inside the allowable range of $\pm5\%$. Therefore, provided that the *objective 2* of (4) is fulfilled, the voltages of all buses $\forall\ t\ \in \{0, ..., Horizon\}$ will always lie inside their limits, due to the update of (16).

Step 6: If the *Cost* function is not further reduced, then exit (the optimization is completed). Otherwise, return to step 1.

V. SIMULATION RESULTS

The performance of the proposed optimization approach is investigated in the unbalanced IEEE 8500-node network.

A. Network Description

The topology of the network is shown in Fig. 4. It is a real 4-wire MV network with a phase-to-neutral voltage 7200 V and maximum load 10.7 MW and 2.7 MVar [36]. Data about the network are provided in Table I. The network is considered islanded with a thermal generator, four HPPs, one SVR and one capacitor bank. Data about the maximum and minimum discharge power ($P_{dschrg_i}^{max}, P_{dschrg_i}^{min}$), renewable capacity, maximum apparent power ($S_{hpp_1}^{max}$), charge and discharge efficiency ($\varepsilon_{chrgi}, \varepsilon_{dschrgi}$), maximum and minimum stored energy ($StE_{hpp_i}^{max}, StE_{hpp_i}^{min}$) of HPP $i \in \{1, ..., 4\}$, are given in Table II. In the same table, data about the technical minima of thermal generator, SVR and capacitor bank are quoted. The four HPPs consist of the following renewable and storage systems:

- *HPP 1: Wind Farm 3 MW & CAES 3 MW/10 MWh*
- *HPP 2: Wind Farm 6 MW & PHS 6 MW/20 MWh*
- *HPP 3: Solar Park 1 MW & BSS 1 MW/6 MWh*
- *HPP 4: Solar Park 1 MW & BSS 1 MW/6 MWh*

Due to the fast response of BSSs, the solar generators of HPP 3 and 4 are connected directly to the grid (mode 1 of section II.B). On the opposite, wind farms of HPP 1 and 2 are split (mode 3), so that the 25% of the installed power (namely 0.75MW and 1.5MW for HPP 1 and HPP 2, respectively) is directly connected to the grid, while the 75% is connected to the ESSs. The total load of the network throughout the examined 24-hour horizon is shown in Fig. 5. The power factor of all loads is assumed 0.97 inductive.
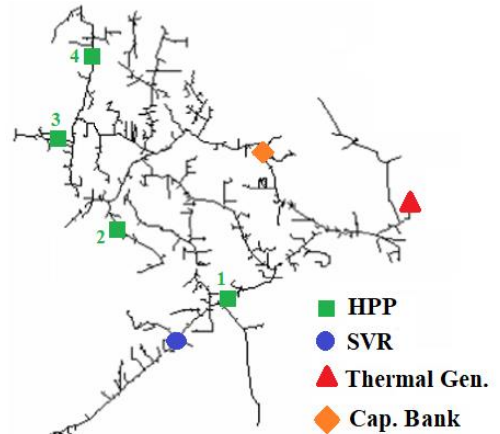
Fig. 4. Modified IEEE 8500-node network, consisting of 1 thermal generator, 4 HPPs, 1 SVR and 1 capacitor bank.
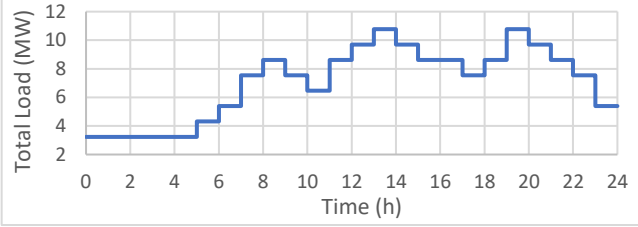
Fig. 5. Total load of the network, during the examined 24-h period. Three peaks are observed: in the morning, in the midday and in the evening.

TABLE I
DATA OF THE IEEE 8500-NODE NETWORK

Line Lengths	Given in [36]
Resistance/Reactance of the lines	Given in [36]
Active power load of each phase	Given in [36]
Total active power load	10.7 MW [36]
Power factor of each phase	0.97 inductive
Phase-to-neutral nominal voltage	7200 V
Maximum voltage limit (+5%)	7560 V
Minimum voltage limit (-5%)	6840 V

TABLE II
DATA ABOUT THE HPP, SVR AND CAPACITOR BANK

$[P_{dschrg_1}^{max} \quad P_{dschrg_2}^{max} \quad P_{dschrg_3}^{max} \quad P_{dschrg_4}^{max}]$	$[3 \quad 6 \quad 1 \quad 1] \, MW$
$[P_{dschrg_1}^{min} \quad P_{dschrg_2}^{min} \quad P_{dschrg_3}^{min} \quad P_{dschrg_4}^{min}]$	$[0 \quad 0 \quad -1 \quad -1] \, MW$
Renewable Nominal Power $[HPP\,1 \quad HPP\,2 \quad HPP\,3 \quad HPP\,4]$	$[3 \quad 6 \quad 1 \quad 1] \, MW$
$[S_{hpp_1}^{max} \quad S_{hpp_2}^{max} \quad S_{hpp_3}^{max} \quad S_{hpp_4}^{max}]$	$[4 \quad 7 \quad 1.5 \quad 1.5] \, MVA$
$[\varepsilon_{chrg1} \quad \varepsilon_{chrg2} \quad \varepsilon_{chrg3} \quad \varepsilon_{chrg4}]$	$[0.85 \; 0.85 \; 0.9 \; 0.9]$
$[\varepsilon_{dschrg1} \quad \varepsilon_{dschrg2} \quad \varepsilon_{dschrg3} \quad \varepsilon_{dschrg4}]$	$[0.85 \; 0.85 \; 0.9 \; 0.9]$
$[StE_{hpp_1}^{min} \quad StE_{hpp_2}^{min} \quad StE_{hpp_3}^{min} \quad StE_{hpp_4}^{min}]$	$[1 \quad 1 \quad 1 \quad 1] \, MWh$
$[StE_{hpp_1}^{max} \quad StE_{hpp_2}^{max} \quad StE_{hpp_3}^{max} \quad StE_{hpp_4}^{max}]$	$[10 \quad 20 \quad 6 \quad 6] \, MWh$
Technical minima of thermal DG (TechLim)	*1 MW*
SVR step range ($Tap_k^{min}, \ldots, Tap_k^{max}$)	$[-16, \ldots 0, \ldots 16]$
Maximum step-up (down) voltage of SVR	*± 10%*
Step size of SVR (dTap)	*0.00625*
Configuration of SVR	*wye*
Step size of Capacitor Bank (dCap)	*20 μF*
Maximum Capacitance of Capacitor Bank (Cap_l^{max})	*120 μF*

B. Scenario 1 (high renewable generation)

In the first scenario, we test our approach in a day where the renewable's generation is high. The total generation of renewable's parks of the four HPPs is shown in Fig. 6. As shown, the wind generators of HPP 1 and HPP 2 operate above 2 MW and 4 MW, respectively, for the time interval between 5.00-21.00, and in their maximum powers (3MW and 6MW) during the time interval 15.00-16.00 h. The solar generators of HPP 3 and HPP 4 reach their maximum powers (1MW) in the midday. The initial stored energy (at t=0) of the four HPPs is $[StE_{hpp_1}(0) \; StE_{hpp_2}(0) \; StE_{hpp_3}(0) \; StE_{hpp_4}(0)] = [5 \quad 10 \quad 4 \quad 4] \, MWh$, where $StE_{hppi}(t)$ is the stored energy of HPP i at time *t*.

The direct penetration of renewables of HPPs is depicted in Fig. 7 calculated by the set of equations (1). It is observed that the solar energy of HPP 3 and HPP 4 is totally injected in the network, due to the fast response of BSS that can quickly compensate rapid variations of solar energy, ensuring the stability of the network, as explained in Section II. On the other hand, in HPP 1 and 2, only the 25% of wind energy is directly injected in the network, as calculated by (1) setting $\alpha_{dpi} = 0.25$ for $i=\{1,2\}$. In the same figure, it is noticed that a small portion

of the directly injected wind power of HPP 1 and HPP 2 is curtailed, in the first 6 hours. This is due to the low dynamic RES penetration limit, as a result of the low load of the network.

The charge powers of the storage systems of HPP 1 and 2 are shown in Fig. 8. The charge power of the energy storage systems of HPPs is calculated by (2). Although some wind power is lost by the charging and discharging of ESSs, the total power generation of HPPs 1 and 2 is significantly higher, due to the very low wind curtailments.

The discharge powers of all HPPs are shown in Fig. 9. A negative power of HPP 3 and 4 denote charging of battery. It is confirmed from the figure that the maximum and minimum discharge powers defined in Table II ($P_{dschrg_i}^{max}$, $P_{dschrg_i}^{min}$) are all satisfied. The stored energy of storage systems of HPPs is shown in Fig. 10. The maximum and minimum stored energy defined in Table II ($StE_{hpp_i}^{min}, StE_{hpp_i}^{max}$) are all satisfied $\forall \, i \in \{1, \ldots, 4\}$.

The reactive powers of HPPs, the taps of SVR and the steps of capacitor bank are shown in Figs. 11, 12 and 13, respectively. In all cases the constraints (12), (14) and (15) are satisfied.

Fig. 14 depicts the generated power of thermal generator during the optimized 24-h period. It is always higher than its technical minima (1 MW), with a production slightly above 1MW (e.g., ~1.5MW), during the peak load hours, reducing significantly, the fossil fuel consumption and carbon dioxide emissions. Therefore, it is confirmed that *objective 1* in eq. (4) has been successfully achieved.

Fig. 15 illustrates the maximum and minimum voltages of the network, during the optimized 24-h period. The thermal generator's voltage, as it is calculated by (16), is depicted in Fig. 16. As shown, the maximum and minimum voltage limits, defined in Table I, are all fulfilled. Consequently, it is confirmed that *objective 2* of eq. (4) is successfully satisfied.

Finally, in order to highlight the importance of Volt/Var control in distribution networks, we execute the optimization problem by setting $c_{obj2} = 0$. Practically, it means that only the *objective 1* is minimized by the cost function (4), neglecting the *objective 2*. The voltage profile of this case is shown in Fig. 17, where overvoltages and undervoltages exist beyond 8200 V and 6200 V, respectively, which are far away from the ±5% voltage limits.
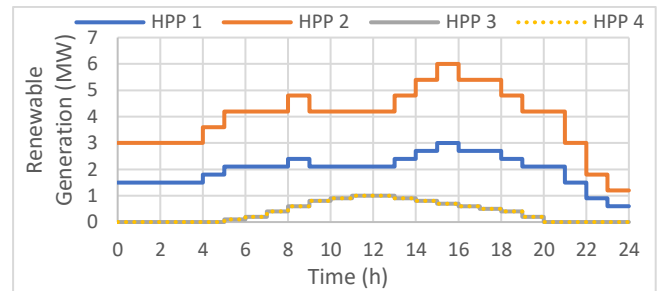
Fig. 6. Generation of renewables of HPPs, during the examined 24-h period, for scenario 1.
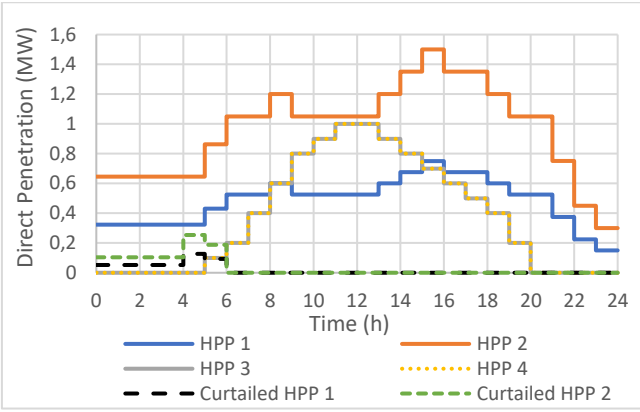
Fig. 7. Direct penetration of renewables of HPPs during the examined 24-h period, for scenario 1.
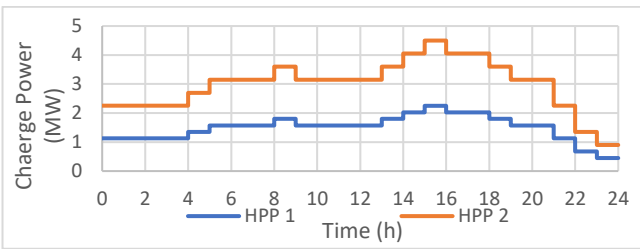
Fig. 8. Charge power of the storage systems of HPPs, during the examined 24-h period, for scenario 1.
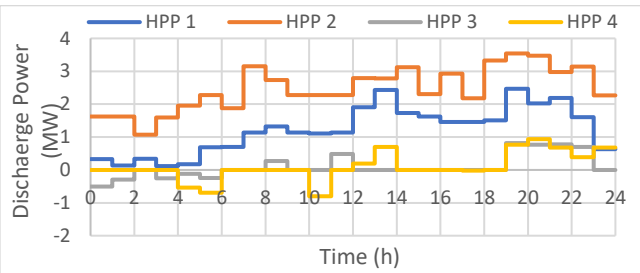
Fig. 9. Discharge power of the storage systems of HPPs, during the examined 24-h period, for scenario 1.
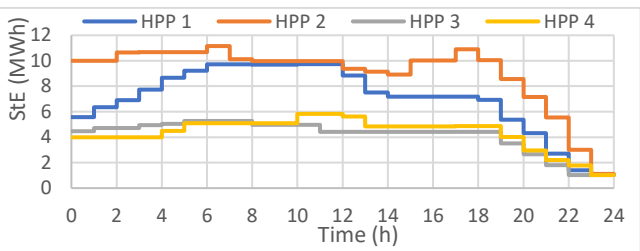
Fig. 10. Stored energy (*StE*) of storage systems of HPPs, during the examined 24-h period, for scenario 1.
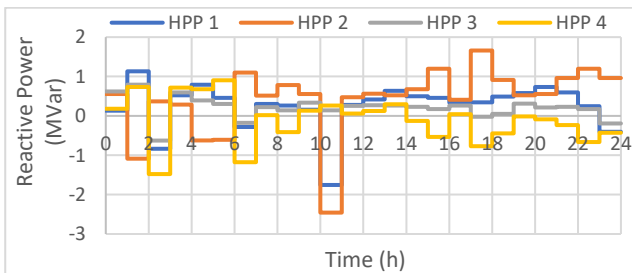
Fig. 11. Reactive power of HPPs, during the examined 24-h period, for scenario 1.
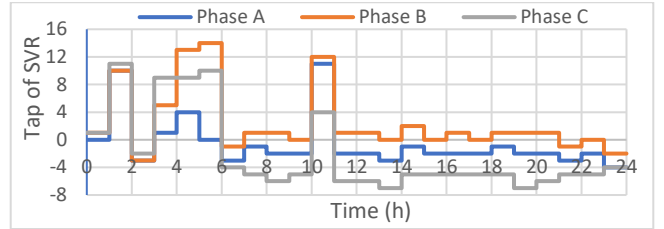
Fig. 12. Taps of SVRs, during the examined 24-h period, for scenario 1.
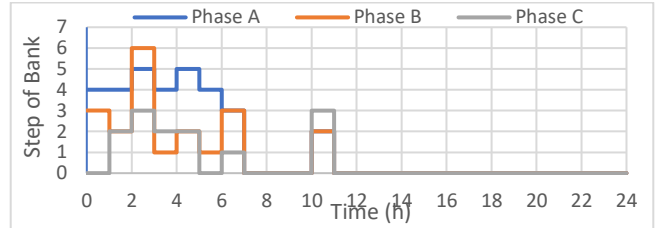
Fig. 13. Step of capacitor banks, during the examined 24-h period, for scenario 1.
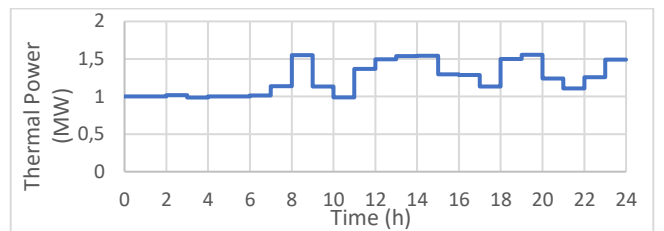
Fig. 14. Generated power of thermal generator, during the examined 24-h period, for scenario 1.
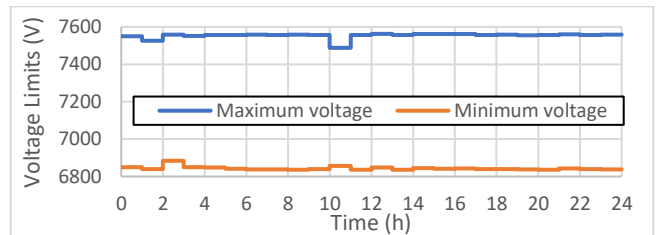
Fig. 15. Maximum and minimum voltage of the network, during the examined 24-h period, for scenario 1.
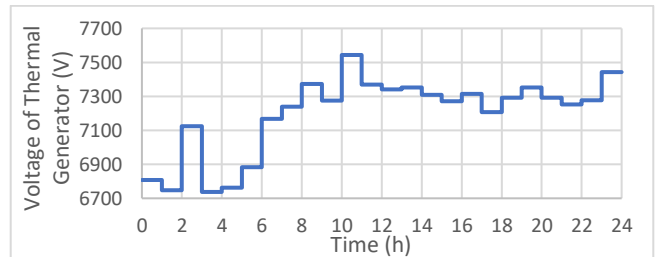
Fig. 16. Voltage of thermal generator, calculated from (16), during the examined 24-h period, for scenario 1. Thermal generators have the capability to regulate their voltage through AVRs.
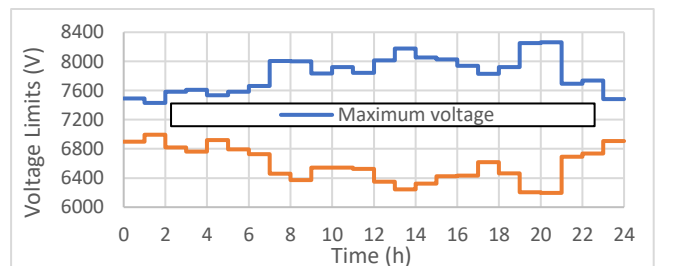
Fig. 17. Maximum and minimum voltage of the network, during the examined 24-h period, for scenario 1. The penalty coefficient c_{obj2} in (4) is set to zero, deactivating the volt/var control.

C. Scenario 2 (low renewable generation)

In the second scenario, we test our approach in a day where the wind generation is zero, while the maximum solar generation, at the midday, is 50% of the nominal value. The load is the same with scenario 1 (see Fig. 5). The initial stored energy (at t=0) of the four HPPs is $[StE_{hpp_1}(0) \ StE_{hpp_2}(0) \ StE_{hpp_3}(0) \ StE_{hpp_4}(0)] =$ [10 20 6 6] MWh. In this scenario the charge power of HPPs is zero, due to the negligible renewable generation. Moreover, although the power of thermal generator is successfully minimized through the *objective 1* of (4), its value is significantly higher than scenario 1, due to the negligible renewable generation.

The discharge power and stored energy of HPPs is shown in Fig. 18 and 19, respectively. All the constraints are fulfilled, although they are not depicted here, due to space limitation. As shown, HPPs are discharged in hours of peak demand e.g., at 8.00, 13.00, 19.00, allocating optimally, the available stored energy along the 24-hour period. The optimal allocation of stored energy is performed in step 4 of Section IV.E and results in a better voltage profile, lower power losses and less loading of conductors. Based on the simulations, the optimal allocation of stored energy causes a daily power loss reduction up to 2 MWh, compared to the case where the stored energy is exploited, at each time instant, to the maximum possible extent, ignoring the future energy needs of the network.
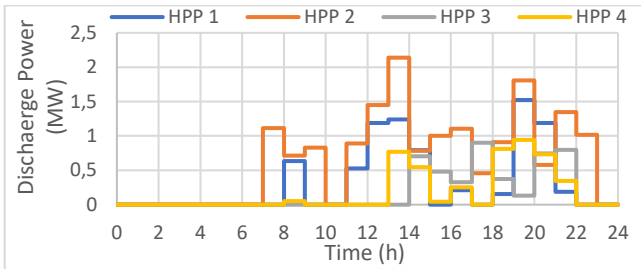
Fig. 18. Discharge power of the storage systems of HPPs, during the examined 24-h period, for scenario 2.
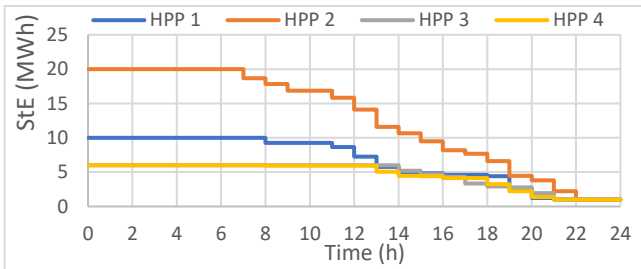
Fig. 19. Stored energy (*StE*) of storage systems of HPPs, during the examined 24-h period, for scenario 2.

D. Scalability of the Proposed Optimization Approach

The computation time of the proposed approach is investigated here, for the high renewable scenario (scenario 1) using the IEEE 8500-Node network with a different number of HPPs. In the first case, the network includes 4 HPPs, 1 SVR and 1 capacitor bank, with the data of Table II. The second case includes 8 HPPs, 1 SVR and 1 capacitor bank. The third case includes 12 HPPs, 1 SVR and 1 capacitor bank distributed uniformly in the network. In all cases, the total storage capacity and installed capacity of renewables is the same. All simulations were executed in a PC with a 64-bit Intel Core i7, 3.4 GHz CPU and 16GB RAM. The required repetitions (namely from step 1 to step 6 in section IV.E), the computation

time per repetition and the total computation time are given in Table III, for all the cases. As shown, for the case of 4 HPPs, the proposed approach requires around 70 repetitions to minimize the cost function (4), and a total computation time of 600 seconds. Given the large size of the network and the precise three-phase representation, we believe that this time is absolutely reasonable, enabling the real-time applicability of the approach. The longest time is required for the case of 12 HPPs, where the computation time is about 2000 seconds (around 30 minutes). Even in that case, the computation time remains reasonable given the large number of optimization variables and large size of the network.

TABLE III
COMPUTATION TIME OF THE PROPOSED APPROACH, FOR DIFFERENT NUMBERS OF HPPS, IN THE IEEE 8500-NODE NETWORK

No. of HPPs	Required repetitions	Time per repetition	Computation time
4	~70	~9 sec	~600 sec
8	~110	~13 sec.	~1400 sec.
12	~ 120	~17 sec	~2000 sec

E. Comparison Against Other Optimization Methods

Heuristic optimization algorithms such as particle swarm optimization (PSO) are not applicable in such large networks with long time horizons, due to the extremely long computation time. As an example, assuming that each particle is associated with a cost value of (4), it will require the solution of power flow for the 24-hour horizon, namely 24 power flow solutions. Each power flow, for the IEEE 8500-node network, is solved in around 2 seconds, using the implicit Z-Bus method of [35]. As a result, the cost value of each particle would be calculated in around 2·24=48 seconds. Considering 50 particles, which converge to around 30 iterations, the total computation time of PSO would be around 50·30·48s=72000 seconds ≈ 20 hours. This time is extremely high, making PSO method practically inapplicable.

Additionally, the use of MINLP is characterized by prohibitive execution time due to the extremely large size of the examined network. Specifically, the 24-hour optimization problem for the IEEE 8500-node network was mathematically formulated in GAMS, a powerful optimization software, which was unable to return a feasible solution even after 10 days. The main reason behind this lies on the extreme size of the problem, which consists of 786816 variables, 725923 equality constraints and 484032 inequality constraints, making the finding of optimal solution using MINLP practically infeasible. The GAMs implementation and the respective MATLAB code of MINLP can be found in the following link:

https://www.dropbox.com/s/x9r94t0941pyox7/OPF.zip?dl=0

VI. CONCLUSION

This paper proposes a sensitivity-based optimization approach for performing, simultaneously, energy management and three-phase volt/var control in non-interconnected insular systems with multiple hybrid power plants. More specifically, the method calculates, for a period of 24 hours, the optimal active and reactive powers of HPPs, the states of SVRs and capacitor banks, as well as the voltage of thermal generator in order to minimize the generation cost of thermal generators, while at the same time, satisfying the following constraints: a) the technical limits of diesel generators, b) the maximum direct

penetration limits of renewables, c) the state of charge limits of energy storage systems, d) the three-phase voltage limits of all the buses of the network. According to the simulations, the proposed method successfully achieves the aforementioned objectives. In contrast to the existing optimization methods e.g., PSO, MINLP, which are practically inapplicable in large networks with long optimization horizons, the proposed method presents a reasonable computation time. A summary of the main advantageous characteristics of the proposed approach compared with other existing methods is provided in Table IV at the end of the paper.

REFERENCES

[1] D. A. Katsaprakakis et. Al., "Comparing electricity storage technologies for small insular grids", Applied Energy, 113332, Volume 251, 2019.

[2] D. Katsaprakakis et. Al, "Hybrid power plants in non-interconnected insular systems", Applied Energy, Volume 164, Pages 268-283, 2016.

[3] I. D. Margaris et. Al., "Frequency control in autonomous power systems with high wind power penetration", IEEE Trans. Sustain. Energy, vol. 3, no. 2, pp. 189-199, Apr. 2012.

[4] Sebastian Braun, "Improving Flexibility of Fossil Fired Power Plants", Encyclopedia of Energy Storage, Vol. 2, Pages 133-140, 2022.

[5] Kaldellis, J.K. "Supporting the Clean Electrification for Remote Islands: The Case of the Greek Tilos Island", Energies, 14, 1336, 2021,

[6] S. Papathanassiou et. Al., "Power limitations and energy yield calculation for wind farms operating in island systems," Renew. Energy, vol. 31, no. 4, pp. 457–479, Apr. 2006.

[7] K.A Kavadias, et. Al., "Modelling and optimisation of a hydrogen-based energy storage system in an autonomous electrical network", Applied Energy 227, pp. 574-586, 2017.

[8] D.A. Katsaprakakis et. Al., "A Multidisciplinary Approach for an Effective and Rational Energy Transition in Crete Island, Greece", Energies, 15, 3010, 2022.

[9] R. A. Jabr et. Al., "Sensitivity-based discrete coordinate-descent for Volt/VAr control in distribution networks", IEEE Trans. Power Syst., vol. 31, no. 6, pp. 4670-4678, Nov 2016.

[10] A. Borghetti, "Using mixed integer programming for the volt/VAr optimization in distribution feeders", Elect. Power Syst. Res., vol. 98, pp. 39-50, May 2013.

[11] S. Zhan et. Al., "Co-optimized trading of hybrid wind power plant with retired EV batteries in energy and reserve markets under uncertainties", International Journal of Electrical Power & Energy Systems, Volume 117, 105631, 2020.

[12] G. N. Psarros et. Al., "Feasibility analysis of centralized storage facilities in isolated grids", IEEE Trans. Sustain. Energy, vol. 9, no. 4, pp. 1822-1832, Oct. 2018.

[13] G. Agundis-Tinajero et al., "Extended-optimal-power-flow-based hierarchical control for islanded AC microgrids", IEEE Trans. Power Electron., vol. 34, no. 1, pp. 840-848, Jan 2019.

[14] E. R. Sanseverino et. Al., "Optimal power flow in three-phase islanded microgrids with inverter interfaced units", Electric Power Systems Research, Volume 123, Pages 48-56, 2015.

[15] M. Marzband et. Al,, "An optimal energy management system for islanded microgrids based on multiperiod artificial bee colony combined with markov chain", IEEE Syst. J., vol. 11, no. 3, pp. 1712-1722, Sep. 2017.

[16] B. Zhao et. Al., "Operation optimization of standalone microgrids considering lifetime characteristics of battery energy storage system", IEEE Trans. Sustain. Energy, vol. 4, no. 4, pp. 934-943, Oct. 2013.

[17] R. Palma-Behnke et al., "A microgrid energy management system based on the rolling horizon strategy", IEEE Trans. Smart Grid, vol. 4, no. 2, pp. 996-1006, Jan. 2013.

[18] D. E. Olivares, C. A. Cañizares and M. Kazerani, "A centralized energy management system for isolated microgrids", IEEE Trans. Smart Grid, vol. 5, no. 4, pp. 1864-1875, Jul. 2014.

[19] X. Wu et. Al., "A hierarchical framework for generation scheduling of microgrids", IEEE Trans. Power Del., vol. 29, no. 6, pp. 2448-2457, Dec. 2014.

[20] P. P. Vergara et al., "Optimal operation of unbalanced three-phase islanded droop-based microgrids", IEEE Trans. Smart Grid, vol. 10, no. 1, pp. 928-940, Jan. 2019.

[21] P. P. Vergara et. Al., "A generalized model for the optimal operation of microgrids in grid-connected and islanded droop-based mode", IEEE Trans. Smart Grid, vol. 10, no. 5, pp. 5032-5045, Sep. 2019.

[22] Y. Vilaisarn et. Al., "An MILP formulation for the optimum operation of AC microgrids with hierarchical control", International Journal of Electrical Power & Energy Systems Volume 137, 107674, 2022.

[23] Y. Levron et. Al., "Optimal power flow in microgrids with energy storage", IEEE Trans. Power Syst., vol. 28, no. 3, pp. 3226-3234, Aug. 2013.

[24] A. Maulik et. Al., "Optimal operation of droop-controlled islanded microgrids", IEEE Trans. Sustain. Energy, vol. 9, no. 3, pp. 1337-1348, Jul. 2018.

[25] S. Conti et. Al., "Optimal dispatching of distributed generators and storage systems for MV islanded microgrids", IEEE Trans. Power Del., vol. 27, no. 3, pp. 1243-1251, Jul. 2012.

[26] H. Mahmood et. Al., "Autonomous Power Management of Distributed Energy Storage Systems in Islanded Microgrids", IEEE Transactions on Sustainable Energy, Vol. 13, Issue: 3, 2022.

[27] Frank, S., Steponavice, I. & Rebennack, S. Optimal power flow: a bibliographic survey I. Energy Syst 3, 221–258 (2012). https://doi.org/10.1007/s12667-012-0056-y

[28] A. F. Guillamón et. AL., "Analysis of power system inertia estimation in high wind power plant integration scenarios", IET Renewable Power Generation, Vol. 13, Issue 15, Pages 2807-2816, 2019.

[29] S. V. Papaefthymiou et. Al., "Dynamic analysis of island systems with wind-pumped-storage hybrid power stations", Renewable Energy, Volume 74, Pages 544-554, 2015.

[30] M. Kendall et. Al,. "An Evaluation of Energy Storage Cost and Performance Characteristics" Energies, no. 13(13):3307, 2020.

[31] N. Psarros et. Al., "Internal dispatch for RES-storage hybrid power stations in isolated grids", Renewable Energy, Volume 147, Part 1, Pages 2141-2150, 2020.

[32] Thomas Allen Short, "Electric Power Distribution Equipment and Systems", Taylor & Francis eBooks, Copyright Year 2005.

[33] E. E. Pompodakis et. Al. "A comprehensive three-phase step voltage regulator model with efficient implementation in the Z-bus power flow", Electric Power Systems Research, Volume 199, 107443, 2021.

[34] NEPSI, Northeast Power Systems Inc, "Step and Stage Size Considerations", Accessed on: July 15, 2022. [Online]. Available: https://nepsi.com/resource/Step%20and%20Stage%20Sizes.pdf

[35] E. E. Pompodakis et. Al., "A generic power flow algorithm for unbalanced islanded hybrid AC/DC microgrids", IEEE Trans. Power Syst., vol. 36, no. 2, pp. 1107–1120, 2021.

[36] IEEE PES. (2022, July) Distribution test feeders, "8500-Node Test Feeder". [Online]. Available: http://www.ewh.ieee.org/soc/pes/dsacom/testfeeders/index.html

[37] F. Olivier et. Al., "Modelling of three-phase four wire low voltage cables taking into account the neutral connection to the earth", CIRED Workshop - Ljubljana, 7-8, Paper 0593, June 2018.

[38] M. Z. Kamh et. AL., "Three-phase steady-state model of type-3 wind generation unit—Part II: Model Validation and Applications", IEEE Trans. Sustain. Energy, vol. 3, no. 1, pp. 41-48, 2012.

[39] A. V. Ntomaris et. AL., "Stochastic scheduling of hybrid power stations in insular power systems with high wind penetration", IEEE Trans. Power Syst., vol. 31, pp. 3424-3436, 2016.

[40] Law 4414/2016, https://www.e-nomothesia.gr/energeia/nomos-4414-2016.html, in Greek language.

[41] Kendall Mongird et. Al., "Grid Energy Storage Technology Cost and Performance Assessment", Technical Report, US Department of Energy, Publication No. DOE/PA-0204, December 2020.

[42] A. Fernández-Guillamón et. Al., "Frequency control studies: A review of power system, conventional and renewable generation unit modeling", Electric Power Systems Research, Volume 211, 108191, 2022.

[43] Lukas Sigrist et. Al., "A review of the state of the art of UFLS schemes for isolated power systems", International Journal of Electrical Power & Energy Systems, Volume 99, Pages 525-539, 2018.

[44] S. M. Muyeen et. Al., "Electrolyzer switching strategy for hydrogen generation from variable speed wind generator", Electric Power Systems Research Volume 81, Issue 5, Pages 1171-1179, 2011.

[45] N. Nguyen and J. Mitra, "An analysis of the effects and dependency of wind power penetration on system frequency regulation", IEEE Trans. Sustain. Energy, vol. 7, no. 1, pp. 354-363, Jan. 2016.

[46] José Ignacio Sarasúa et. AL., "Analysis of alternative frequency control schemes for increasing renewable energy penetration in El Hierro Island power system", International Journal of Electrical Power & Energy Systems, Volume 113, Pages 807-823, 2019.
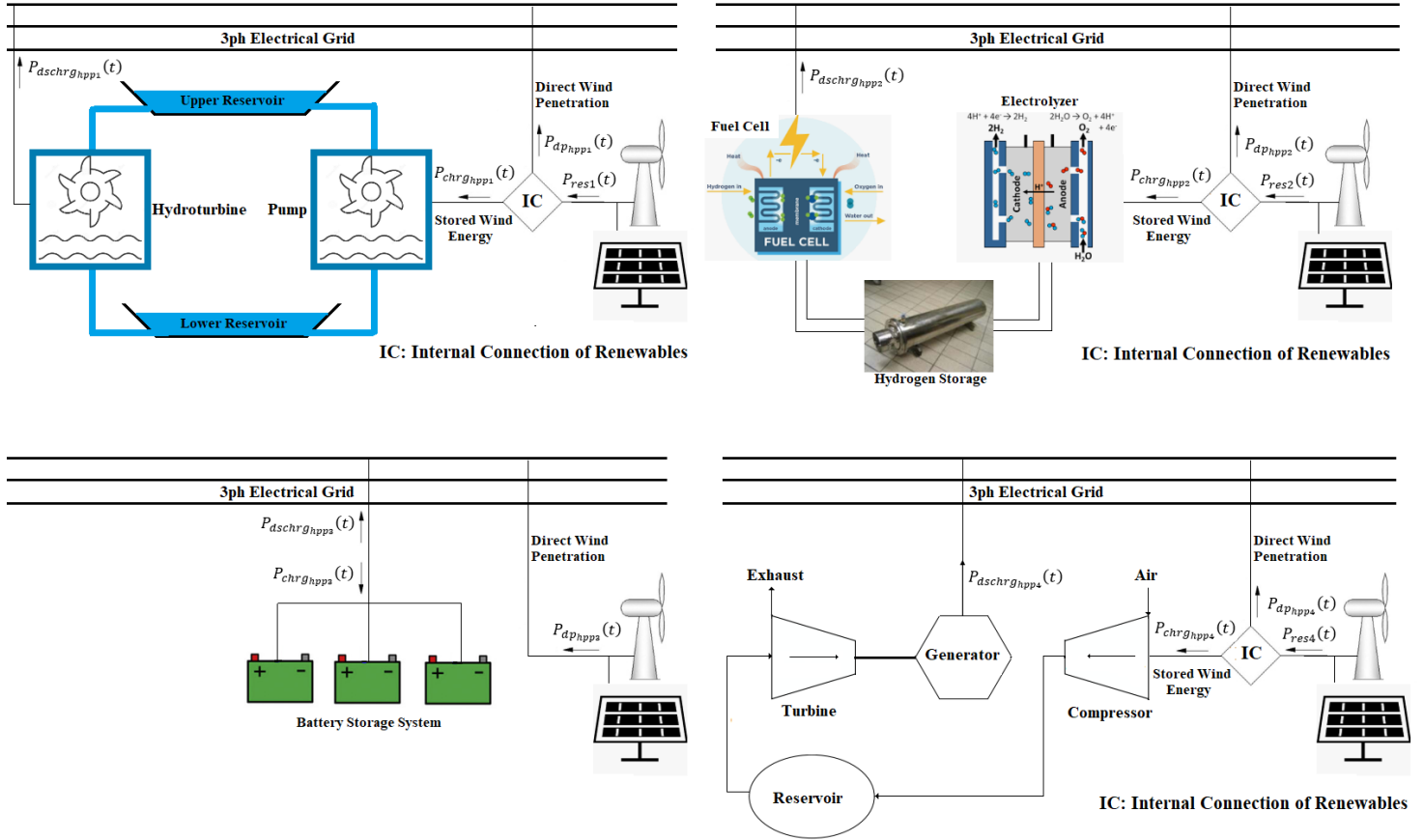
Fig. 1. Types of hybrid power plants. 1a) Top-left (HPP-PHS): RESs with pumped storage, 1b) Top-right (HPP-HSS): RESs with Hydrogen storage, 1c) Bottom-left (HPP-BSS): RESs with battery storage, 1d) Bottom-right (HPP-CAES): RESs with compressed air energy storage.

TABLE IV
OVERALL COMPARISON BETWEEN THE PROPOSED APPROACH AND OTHER EXISTING APPROACHES

	Energy management	Volt/var Control	Technical Limits of Thermal Generators	Consideration of SVRs, Cap. banks	Dynamic stability limits	Accurate Modelling of HPPs	Computation time	1 phase / 3 phases
Refs. [1], [2]	✓	✗	✓	✗	✓	✓	Low	NEA*
Ref. [9]	✗	✓	✗	✗	✗	✗	Low	1 phase
Ref. [10]	✗	✓	✗	✗	✗	✗	Medium	1 phase
Ref. [12]	✓	✗	✓	✗	✓	✓	Low	NEA*
Refs. [13] [14]	✗	✓	✗	✗	✗	✗	Low	3 phases
Refs [15] - [17]	✓	✗	✗	✗	✗	✗	Low	NEA*
Refs. [18] – [22]	✓	✓	✗	✗	✗	✗	Medium	3 phases
Ref. [23]	✓	✓	✗	✗	✗	✗	High	3 phases
Ref. [24] [25]	✓	✓	✗	✗	✗	✗	Very high	1 phase
Ref. [26]	✓	✗	✗	✗	✗	✗	Low	NEA*
Proposed	✓	✓	✓	✓	✓	✓	Low	3 phases

*NEA: None Electrical Analysis